Forces on an intruder combining translation and rotation in granular media

Antoine Seguin

Forces on an intruder combining translation and rotation in granular media

A. Seguin[1]
[1] *Université Paris-Saclay, CNRS, FAST, 91405 Orsay, France*

An investigation of the mechanical actions on a moving intruder into a granular medium subjected to a gravity field is provided using two dimensional numerical simulation. The interactions between the grains are frictionless and modeled by Hertz's law with a viscous damping. The intruder has a cross-shaped geometry and was initially buried at a shallow depth. It has the ability to translate and rotate at constant velocities independently of each other, thus defining a translational Froude number Fr and a rotational Froude number Γ. We study the evolutions of the drag force D_x, the lift force L_y and the torque M_z exerted on the intruder. In the case of pure horizontal translation with a low Froude number, these quantities are constant and independent of Fr with $M_z = 0$. In the case of pure rotation leading to $D_x = 0$, the torque is constant when $\Gamma \to 0$ and increases with Γ. For the combination of translation and rotation, we also determine the evolutions laws of the mechanical actions with Γ: the rotation generates an increase of the torque on the intruder while the drag force decreases. We highlight the existence of a significant drop of the lift force favouring the anchoring of the intruder in the granular medium for a specific range of Γ. By applying the granular resitive force theory, we determine theoretical expressions to describe the evolution of the drag force D_x and the torque M_z. The theoretical results are in agreement with the simulation results.

I. INTRODUCTION

In the 2000s, a small lizard, called sandfish, was popularized by an experimental study highlighting its ability to swim and evolve in the sand [1]. Animal locomotion over the surface of a granular medium or inside the granular medium itself remains a source of inspiration for scientific projects since the associated movements are generally optimized [2–4]. Understanding the mechanical behaviors of animals in order to be able to reproduce them in the eventuality of designing bio-inspired machines or robots remains an exciting challenge. Thus, an experimental study on a model robot able to move thanks to a propeller was recently developed: the realized movement allowed a translation with an axial rotation like an Archimedes' screw [5]. At the same time, many scientific studies tried to to decompose the different movements that participate to locomotion in granular media and to measure their mechanical responses.

The first elementary movements of objects (or intruders) reported in granular media are most often translational movements. These translational motions of intruders can be vertical, i.e. in the direction of gravity g, generating an unsteady flow of grains. These unsteady flows are present in the case of object impact on a granular medium where the initial energy of the object decreases during the motion [6–11] and dynamic uplift test [12]. Several experimental studies have also explored the case of stationary flow, often generated by a vertical translation at constant velocity of an object in the granular medium. These studies have, for example, highlighted the grain fields [13–15] or the force of resistance to penetration [16, 17]. In the case of horizontal translational motions, i.e. perpendicular to the direction of gravity g, there are numerous experimental and numerical studies dealing with constant velocity displacement V_0 [18–23] and dynamic testing [24]. Through these studies, it is often reported the existence of two regimes which are the two extreme values of a Froude number often defined by $Fr = V_0/(gh)^{1/2}$, where h defines the depth at which the object is buried [25]. The major difference between these two regimes lies in the scaling of the drag force, which corresponds to the resistance to motion, parallel to the movement. For low Froude numbers, i.e. $Fr \ll 1$, the drag force on an object is independent of the translation velocity and scales roughly with the hydrostatic pressure related to the depth of burial of the object, i.e. the weight of the grain column above it [18, 20, 21, 23]. For high Froude numbers, i.e. $Fr \gg 1$, the drag force varies as a quadratic function of velocity scaling as ${V_0}^2$ [19, 22]. In this regime, collisions between grains, of density ρ, generate a kinetic pressure scaling as $\rho {V_0}^2$ which is at the origin of the drag force [26]. Modeling the lift force in granular materials remains challenging. For example, it has been shown that the lift force on a plate could be positive or negative depending on its orientation [27]. More generally, the lift force does not have similar scaling laws as the drag force since it seems to evolve with the Froude Fr number, the depth of burial and its geometric aspect [28].

Unlike translation, the rotational movements of objects in granular media have been less studied. Stirring a granular medium with an object rotation causes a drop in the drag force [29]. In order to limit the fluctuations in lift force, it is necessary that the intruder is sufficiently buried. According to a previous study [30], the origin of the lift force comes from the pressure gradient on the intruder due to gravity at great depths. This pressure gradient generates an asymmetrical distribution of normal stress on the object and creates the lift force. An other study [31] indicates that this same pressure gradient is rather the consequence of a volume fraction

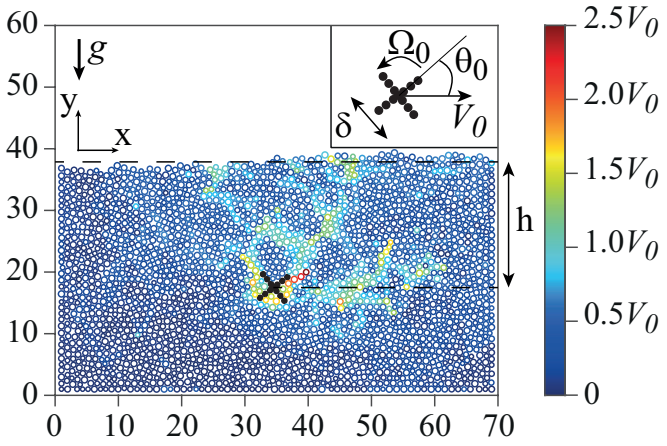

FIG. 1. (Color online) Snapshot of a simulation during the displacement of the intruder moving through a granular medium at $Fr \simeq 0.02$ et $\Gamma \simeq 0.05$ along the x-direction. The intruder is initially buried at depth h. The scales in x and y axis are in grain diameter. Inset: close up of the intruder in its initial position defining its size δ with the spatial organization of the grains, the initial angle θ_0, its linear velocity V_0 and its rotationnal velocity Ω_0. The colour of the grains represents the norm of their velocity vector associated with the selected time according to the displayed color scale.

gradient caused by the shear and the dilation. Recently, a numerical study with high Froude number frictional grains, i.e. without gravity, revealed the Magnus effect exists in granular media [32]. Finally, the origin of the lift force in granular media is still a subject of debate.

In this paper, we study the set of mechanical actions exerted on a cross-shaped intruder, translating horizontally in a granular medium and being able to rotate around its center. We thus characterize the drag force, the lift force and the torque exerted on the intruder as a function of the kinematic parameters of the object's motion. The intruder is initially buried at a shallow depth. First, we briefly describe the numerical method used and we define the set of useful parameters. Then, we carry out a first study on horizontal translation without rotation. Then, the second study focuses on the pure rotation of the intruder without translation. The third study presents the results on the combination of translation and rotation. Finally, we discuss the results in the framework of the Granular Resistive Force Theory.

II. NUMERICAL SETUP AND CONFIGURATION

The numerical method has alredy been used for other analysis [9, 23]. To simulate the displacement of an intruder buried in a two-dimensional granular medium, we use a molecular dynamic method. The typical geometry of the intruder and granular medium is shown in figure 1. The 2D granular medium consists of spheres whose centers are coplanar. The diameters of these spheres can vary between $0.8d$ and $1.2d$ where $d = 1$ mm is the average diameter of the spheres. In order to avoid crystallisation of the packing, we have chosen a uniform distribution of these diameters. All grains have the same mass m, thus defining the average density $\rho = 10^3$ kg.m^{-3}, based on the average diameter d. All grain interactions in the simulation are modelled with a dissipative Hertz law of the form $F_{ij} = k\zeta^{3/2} - \lambda\frac{d\zeta}{dt}$ where ζ is the interpenetration of the grains, k is the stiffness of the contact and λ is a damping coefficient. The stiffness k is related to the Young's modulus $E = 1$ GPa of the grains such as $k = E\sqrt{d/2}$. The coefficient of viscous damping λ simulates a restitution coefficient $e_n = 0.9$. One can notice that the grains are frictionless. The time step is small enough to ensure numerical convergence. The details of these calculations were reported in [9].

The intruder has the shape of a cross in the setup (inset Fig. 1). This arbitrary shape of intruder has been chosen to ensure a dragging of the grains by obstacle during a possible rotation of the intruder since the grains are frictionless. It consists of twelve grains with the same mechanical properties as the granular medium. Therefore the effective diameter δ of this intruder is $\delta = (5+\sqrt{2})d$. Here, the kinematics of these grains constituting the intruder are completely controlled. It is initially buried in the granular medium at a depth $h \simeq 20d$ which is the vertical distance (y-direction) from the upper surface of the granular medium to the center of the intruder (Fig. 1). This upper surface is defined as the average y-position of the grains constituting the higher layer of grains in the initial state. The x position of the intruder in the x-direction corresponds to the horizontal distance from the left wall of the tank to the center of the intruder such that $x = 2.5\delta$ in the initial horizontal position of the intruder (Fig. 1). To prepare for this initial state, the intruder was fixed in his initial buried position. Then, a diluted granular medium is placed above and its sedimentation under the action of gravity ($g = 10$ m.s^{-2} parallel to the y-direction) leads to the initial configuration for further calculations. Once the sedimentation is complete, the tank filling level reaches a finite value that allows us to define h. In this initial organization, the tank containing the product is large enough that the lateral limits ($> 10d$) have no effect on the force exerted on the intruder by the grains [8]. This process leads to an average packing fraction of 0.83. This value is less than the critical volume fraction $\phi_J = 0.85$ indicating that the packing is rigid but still a loose packing [33, 34]. As we use spherical beads of diameter d, the effective length in the third direction is d, so the effective cross section of the intruder scales as δd.

Once the initial configuration has been prepared, we move the intruder at constant velocity V_0 along the x direction (with $\mathbf{e_x}$ the associted unit vector) and 0 along the y-direction (with $\mathbf{e_y}$ the associated unit vector). The in-

truder runs a distance equivalent to 5δ in the x-direction to avoid getting too close to the right wall of the tank [8]. The intruder is initially positioned with an orientation of θ_0. The angle θ_0 represents the angle between the x-direction and the arm of the cross located in the quadrant I (inset Fig. 1).The intruder can also rotate at a rotational velocity Ω_0 around the z-direction, with $\mathbf{e_z}$ the associated unit vector (inset Fig. 1). Similarly to previous studies [25], it is relevant to use the translational Froude number defined by:

$$Fr = V_0/\left(gh\right)^{1/2}. \tag{1}$$

This number links the kinetic pressure $\rho {V_0}^2$ due to collisions [26] and the pressure created by the gravity field ρgh [25]. Taking into account that h is proportional to d, there is then a direct relation between the Froude number Fr and the inertial number I used in the rheological law describing granular materials [35, 36]. Since our problem also presents the phenomenon of pure rotation, it is also possible to define a rotational Froude number by adopting a similar definition. This number can be written as:

$$\Gamma = \delta\Omega_0/\left(gh\right)^{1/2}, \tag{2}$$

since a characteristic linear velocity of rotational motion is $\delta\Omega_0$. These two numbers Fr and Γ are the two control parameters of our study.

During the movement of the intruder at constant velocity V_0 and constant rotation velocity Ω_0, we record the component of the force exerted by the granular medium on the intruder in the x-direction, called drag force, the force exerted by the granular medium on the intruder in the y-direction, called lift force and the torque exerted by the granular medium on the intruder in the z-direction. These mechanical actions are calculated at each time step and are functions of time and contain the collisions between the grains and the intruder. We therefore choose to work with the time averaged quantities once the transitory regime of the translation is over [23]. These temporal averages are calculated once the intruder has crossed a distance equivalent to its diameter δ, which allows to cross the transient regime and to avoid the effects due to the preparation of the packing under the intruder. The drag force (resp. the lift force) is calculated as the sum of the drag (resp. lift) forces on each grain constituting the intruder. The torque is calculated as the sum of the vector products on the grains i constituting the intruder applied to the center of the intruder $\mathbf{r_i} \times \mathbf{F_i}$, where $\mathbf{r_i}$ is the vector linking the center of the intruder to the i grain and $\mathbf{F_i}$ is the force vector applied to that i grain. We call the time averaged drag force $\tilde{D_x}$, the time averaged lift force $\tilde{L_y}$, and the time averaged torque $\tilde{M_z}$. Each observed mechanical action ($\tilde{D_x}$, $\tilde{L_y}$ or $\tilde{M_z}$) also has a characteristic scale in granular materials. Thus the intruder being initially buried at a depth h in all the simulations, a typical pressure scale of the hydrostatic type is ρgh. This pressure is present in many studies [18, 20, 21, 23]. This pressure is applied to a characteristic cross section of the object δd. One builds the dimensionless mechanical actions associated with this scale: the normalized drag force $D_x = \tilde{D_x}/(\rho gh\delta d)$, the normalized lift force $L_y = \tilde{L_y}/(\rho gh\delta d)$ and the normalized torque $M_z = \tilde{M_z}/(\rho gh\delta^2 d)$, using a characteristic lever arm of size δ.

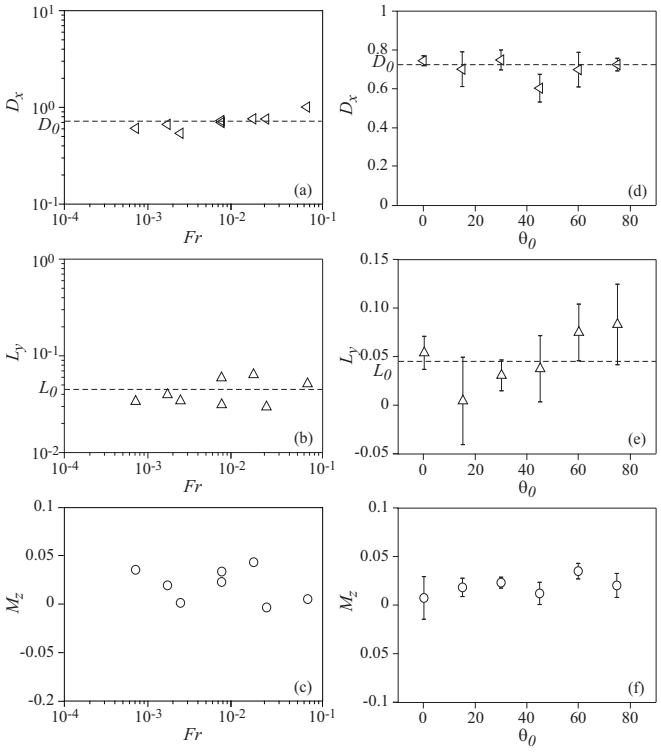

FIG. 2. Evolution of (a) the drag force D_x, (b) the lift force L_y and (c) the torque M_z as a function of translational Froude number Fr. Evolution of (d) the drag force D_x, (e) the lift force L_y and (f) the torque M_z as a function of the initial angle θ_0. The dotted line in (a) and (d) represents the value $D_0 = 0.72$. The dotted line in (b) and (e) represents the value $L_0 = 0.045$ which is the average of the data set of (b) and (e).

The following paper is an analysis of the mechanical actions D_x, L_y and M_z exerted on the intruder as a function of the two control parameters Fr and Γ. The range of variation of Fr is such that $10^{-4} < Fr < 0.3$ even if we will work essentially at $Fr \simeq 0.02$. The range of variation of Γ is such that $-1 < \Gamma < 1$.

III. THE CASE WITH TRANSLATION AND WITHOUT ROTATION: $Fr < 1$ AND $\Gamma = 0$

We first study the classical case of horizontal translation at constant velocity: [18, 20, 21, 23, 27, 28]. The goal here is to validate whether the behavior of the cross-shaped intruder is similar to the disk in the case with no rotation of the intruder, i.e. $\Gamma = 0$. The figure

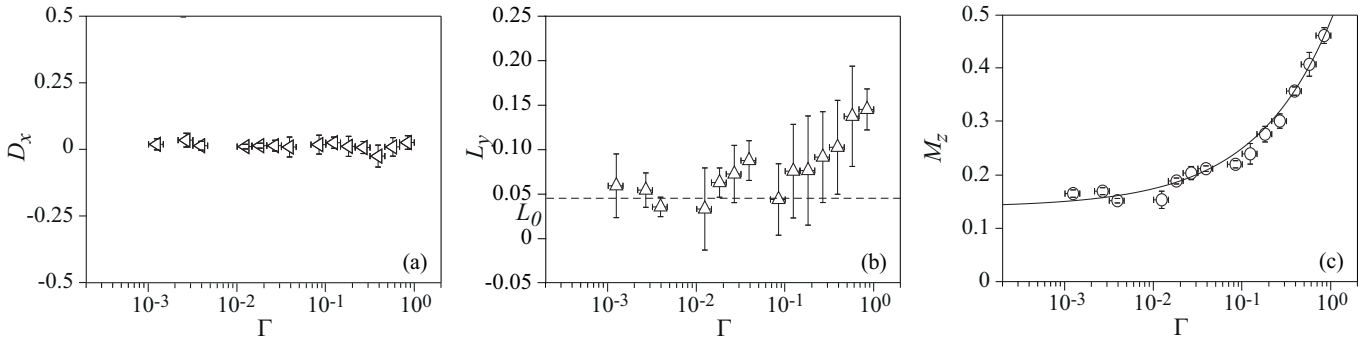

FIG. 3. Evolution of (a) the drag force D_x, (b) the lift force L_y and (c) the torque M_z as a function of rotationnal Froude number Γ. The horizontal dotted line in (b) represents the average value of the lift force $L_0 = 0.045$. The solid line in (c) is given by Eq. 3 with $M_0 = 0.17$, $M_1 = 0.73$ and $\Gamma_0 = 0.76$.

2 presents the various measurements of D_x, L_y and M_z obtained according to the Froude number but also according to the initial orientation angle of the cross, θ_0. The angle θ remains constant such as $\theta = \theta_0$ during the movement since there is no rotation of the intruder.

Figure 2a (resp. b and c) shows the evolution of D_x (resp. L_y and M_z) with the Froude number Fr in the studied range. It is shown that the drag force D_x (Fig. 2a) and the lift force L_y (Fig. 2b) do not evolve significantly with the Froude number. We then consider them as constants. There is no growth of the drag force with Fr^2 here since $Fr \ll 1$ [22, 26]. The influence of the high Froude number on the drag force is not visible. The torque M_z fluctuates with the Froude number Fr with a very low value. This leads us to conclude that $M_z \simeq 0$. Finally, the three mechanical actions (D_x, L_y and M_z) are independent of the Froude numbe in the studied range. To be in this regime, the kinetic pressure $\rho {V_0}^2$ must be lower than the pressure created by the gravity field $\sqrt{\rho g h}$. It is the equivalent of imposing a Froude number $F = V_0/\sqrt{gh}$ smaller than 1. As part of our numerical configuration, it leads to the condition $V_0 \ll 0.5$ m.s^{-1} to ensure that the possible wake created behind the moving intruder is filled [26]. It is also well established that for a small Froude number, the evolution of the drag force on a disk is quasi static [19, 21, 22, 25, 37] and it is then useless to vary this parameter.

Figure 2d (resp. e and f) shows the evolution of D_x (resp. L_y and M_z) with the initial orientation angle θ_0 for $0^\circ \leq \theta_0 < 90^\circ$. Several tests with different packing were performed for each value of θ_0. The results fluctuate and a bar has been added to represent the standard deviation of the measurements for each value of θ_0. The drag force D_x varies little with θ_0 and remains constant (Fig. 2d). This average value is measured to $D_0 = 0.72$ (Fig. 2a and 2d). The torque M_z varies little with θ_0 and we still have M_z which is very close to 0 (Fig. 2f). The lift force fluctuates significantly with θ_0 and the associated standard deviation is not small. We can however estimate an overall average value of the lift force over the data set, this average value is measured to $L_0 = 0.045$ (Fig. 2b and 2e). We find here that the shape of the object influences the lift force, as in the previous studies with comparable dispersion bars and a lift force which can be negative [27, 28, 38].

IV. THE CASE WITHOUT TRANSLATION AND WITH ROTATION: $Fr = 0$ AND $\Gamma < 1$

In this section, we look at the complementary case to the previous one where Fr =0 and $\Gamma \neq$0. Here, there is no translation and rotation is imposed for five rotations of intruder. The transitional regime due to the rotation can be reasonably estimated at one round of intruder [30]. We therefore choose to work with the time averaged quantities once the transitory regime of the rotation is over. Figure 3 shows all the results of this configuration. First we notice that the drag force D_x fluctuates around zero for the whole range of Γ studied so it is reasonable to write that $D_x = 0$ (Fig. 3a). Figure 3c shows the evolution of the torque M_z as a function of Γ. Two regimes can be distinguished: a low value regime of Γ and a high value regime of Γ. In the low Γ regime, the value of M_z is constant. and corresponds to the quasi-static case. In the high Γ regime, the torque M_z increases nonlinearly with Γ. The origin of this torque comes from the effective friction of the granular material on the object. As the flowing properties of the granular material are well described by the $\mu(I)$ rheology [36], we expect to observe a similar rheological law in this flow. In the case of pure rotation of the object around its axis in a granular medium, it is relevant to propose a similar behavior law. Thus we think the best continuous description of the data is

$$M_z(\Gamma) = M_0 + \frac{M_1 - M_0}{1 + \dfrac{\Gamma_0}{\Gamma}}, \qquad (3)$$

with $M_0 = 0.17 \pm 0.01$, $M_1 = 0.7 \pm 0.1$ and $\Gamma_0 = 0.8 \pm 0.2$. In this description, when $\Gamma \to 0$, the torque tends towards

a finite value M_0. This behavior is the complementary case to pure translation where the drag force is not null when $Fr \to 0$ (Fig. 2a).

The figure (Fig. 3b) shows the evolution of L_y with Γ. The value of this lift force is consistent with the values of L_0 measured in figure 2b and 2c (dasehd line). The lift force dispersion bars are still important even if a continuous rotation is imposed here: this is due to the shallow depth of burial. As for the torque M_z, it would appear that a quasi-static regime is emerging for low Γ. In this regime, the value of the lift force is comparable to L_0. Then, in the higher Γ regime, the lift force increases with Γ. Since in this regime the grains above the intruder are relieved of gravity, the lift force comes only from the grains exerted under the intruder. As soon as $\Gamma > 1$, the lift force increases significantly and the torque highly fluctuates, it is the transition to the ballistic regime where no grains are in contact with the intruder. Since this ballistic regime is not the subject of the study, we limit ourselves in the following paper to $\Gamma < 1$.

V. THE CASE WITH TRANSLATION AND ROTATION: $Fr = 0.02$ AND $|\Gamma| < 1$

We now investigate the case where $V_0 \neq 0$ and $\Omega_0 \neq 0$ corresponding to both $Fr \neq 0$ and $\Gamma \neq 0$. However, we have restricted the study to the case of the quasi-static regime in translation, so we keep V_0 constant at 10 mm.s^{-1} leading to $Fr = 0.02$ in this set of simulations. Figure 4 presents the evolution of the drag force D_x, the lift force L_y and the torque M_z applied on the intruder as a function of Γ.

First, we have observed that D_x is an even function of the variable Γ while M_z is an odd function of the variable Γ. In other words, the sign of rotation Ω_0 does not affect the drag force D_x and modifies the sign of the torque M_z. Figure 4a (resp. 4c) shows the evolution of D_x (resp. $|M_z|$) as a function of $|\Gamma|$. We observe that D_x decreases with $|\Gamma|$ (Fig. 4a) and M_z increases with $|\Gamma|$ (Fig. 4c). Here we can identify two regimes. The first regime at small values of $|\Gamma|$ for which the drag force D_x is constant and equal to D_0 and the torque M_z is zero. This velocity corresponds to the fact that the effect of rotation is negligible compared to the effect of translation. The other regime corresponds to larger values of $|\Gamma|$ for which the drag force D_x decreases to near zero and for which the torque $|M_z|$ increases. The increase of the torque with Γ is correlated with the decrease of the drag force D_x. This indicates that there is a transfer of mechanical power from translation to rotation. Moreover, for small values of Γ, the drag force D_x is constant and corresponds to the value D_0 measured for $\Gamma = 0$. For large values of Γ, it seems to be zero. We observe here a transition between these two values of drag force.

Figure 4b shows the evolution of the lift force L_y as a function of Γ. First of all, this function is not monotonous with Γ. We see that for the larger values of Γ, the value of the lift is roughly constant and its value is comparable to the value L_0 found when $Fr = 0$ (Fig. 3b) in the range $\Gamma < 1$. For $\Gamma > 0$, L_y does not exceed L_0 as in the case of pure rotation (Fig. 3b). For $\Gamma < 0$, we observe that $L_y/L_0 > 1$, which shows that the negative sign of rotation amplifies the lift effect compared to values of $\Gamma > 0$. When Γ goes from a negative to a positive value, it seems that the lift L_y decreases sharply to a negative value, passing through a minimum before increasing to positive values. The inset in figure 4b shows a close up on this minimum and displays the evolution of the lift force L_y as a function of $\Gamma/(2Fr)$. For $\Gamma >0$, we see that the lift force decreases with Γ, goes through a minimum and then increases with Γ. We observe that the value of the lift force (positive when $|\Gamma| \to 0$ is in compliance with figures 2b, 2c and 3b). As has already been observed for the lift force, the dispersion of the data is significant. It is thus difficult to give a value to this minimum, however we evaluate it here at $L_m = -0.015 \pm 0.001$. At this minimum, it seems there is a negative lift (or close to 0) and thus the intruder would tend to anchor deeper than its current depth if it was not kept at a constant depth. The value of this minimum is expected to change with depth h. Some simulations have been performed for $h \simeq 100d$ (Fig. 4). Even if the drag force D_x and the moment M_z are independent of h, it is possible that the depth h has an slight influence on the value of the minimum L_m in this configuration (Fig. 4b). The value of this minimum is obtained for $\Gamma_m/(2Fr) \simeq 0.9$ corresponding to $\Gamma_m \simeq 0.036$, taking into account the fact that $Fr = 0.02$. Back to the simulation parameters, that corresponds to $\delta\Omega_0/V_0 \simeq 1.8$ which is very close to the value 2. For this peculiar configuration, the object rolls by pressing slightly the grains above it. Moreover, the rotation induces a fluidization of the granular medium below the intruder which has the effect of reducing the lift action of these grains. The upper part of the granular medium above the intruder is not subject to large grain movements unlike the lower part of the granular medium (Fig. 1). The upper part of the granular medium can apply a greater vertical force on the intruder than the lower part, causing a drop in the lift force.

VI. DISCUSSION

Let us now compare the numerical results to theoretical predicitons. We model the increase of the torque M_z and the fall of the drag force D_x with the rotational Froude number Γ. To do so, we consider the framework of the Granular Resistive Force Theory developed in several studies with the difference that our intruder is not a

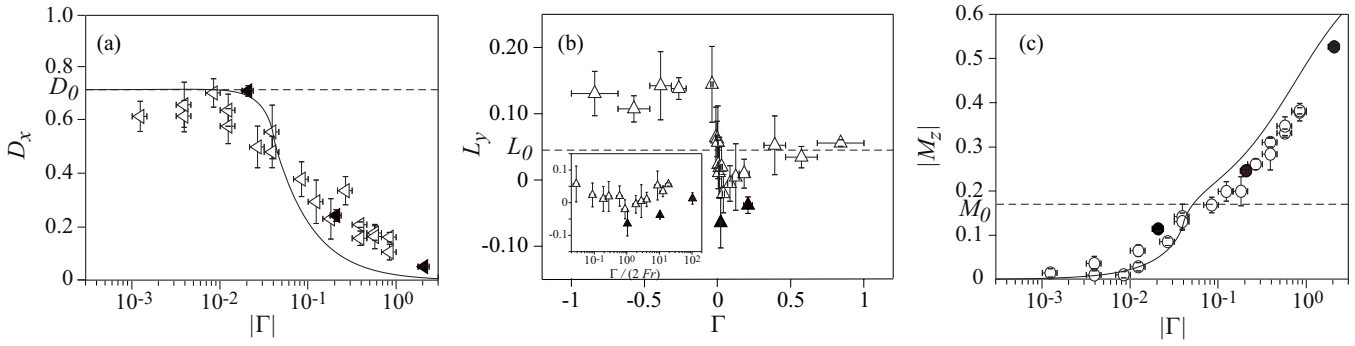

FIG. 4. Evolution of (a) the drag force D_x, (b) the lift force L_y and (c) the torque M_z as a function of rotationnal Froude number Γ for $Fr \simeq 0.02$. The open symbols correspond to $h \simeq 20d$ and the full symbols correspond to $h \simeq 100d$. Inset of (b): lift force L_y as a function of $\Gamma/(2Fr)$. The solid line in (a) represents Eq. 5 and the dotted line represents the value of $D_0 = 0.72$. The dotted line in (b) represents the value of $L_0 = 0.045$. The solid line in (c) represents Eq. 6 and the dotted line represents the value of $M_0 = 0.17$.

slender object [1, 3, 5] or a wheel moving on the surface of a granular medium [39, 40]. We apply a Coulomb-type friction law to the rotating object. Even if it has the shape of a cross, we work as if it were a solid disk of radius $\delta/2$. The frictional force experienced by the intruder is decomposed into a radial force and a tangential force, with two a priori distinct force coefficients C_r and C_α. This model geometry is compatible with a description in a cylindrical coordinate system $(\mathbf{e_r}, \mathbf{e}_\alpha, \mathbf{e_z})$. Thus, the position of a point at the surface of the intruder of radius $\delta/2$ is only defined by an angle α. The velocity of this point during the combined motion is written $\mathbf{v} = (\delta\Omega_0)/2\ \mathbf{e}_\alpha + V_0\ \mathbf{e_x}$. In the framework of Granular Resistive Force Theory, the frictional force per unit length at this point is proportional to the pressure at which the object is buried ($\sim \rho g h$) and is integrated over the thickness ($\sim d$) in the z-direction. This force per unit length can then be written:

$$\mathbf{f} = -\rho g h d \left(C_r \frac{\mathbf{v}\cdot\mathbf{e_r}}{\|\mathbf{v}\|}\mathbf{e_r} + C_\alpha \frac{\mathbf{v}\cdot\mathbf{e}_\alpha}{\|\mathbf{v}\|}\mathbf{e}_\alpha \right), \qquad (4)$$

where C_r and C_α are the normal and tangential effective coefficients of friction. The integration of this force on the surface of the disk of radius δ allows to propose an expression for the drag force D_x (associated to the vector $\mathbf{e_x}$) and the torque M_z (associated to the vector $\mathbf{e_z}$). Thus, we can propose a theoretical expression for the drag force such that:

$$\begin{aligned} D_x =& -\int_0^{2\pi} \frac{\mathbf{f}\cdot\mathbf{e_x}}{\rho g h \delta d}\,\frac{\delta}{2} d\alpha \\ =& \frac{1}{2}\int_0^{2\pi} \frac{-C_\alpha \frac{\Gamma}{2}\sin\alpha + (C_r\cos^2\alpha + C_\alpha \sin^2\alpha)Fr}{\left(Fr^2 + \frac{\Gamma^2}{4} - Fr\Gamma\sin\alpha\right)^{1/2}} \mathrm{d}\alpha. \end{aligned} \qquad (5)$$

We can also propose an expression for the torque such as:

$$\begin{aligned} M_z =& -\int_0^{2\pi} \frac{\left(\frac{\delta}{2}\mathbf{e_r}\times\mathbf{f}\right)\cdot\mathbf{e_z}}{\rho g h \delta^2 d}\,\frac{\delta}{2} d\alpha \\ =& \frac{1}{4}\int_0^{2\pi} \frac{C_\alpha\left(\frac{\Gamma}{2} - \sin\alpha Fr\right)}{\left(Fr^2 + \frac{\Gamma^2}{4} - Fr\Gamma\sin\alpha\right)^{1/2}} \mathrm{d}\alpha. \end{aligned} \qquad (6)$$

The determination of the lift force by this model leads to an expression which will always be equal to 0 in the range of Γ and Fr. This result is a consequence of the Resitive Force Theory model which assumes that the intruder is located at a constant pressure. The model cannot capture the lift evolutions on the object which cannot be considered as slender.

The results for $\Gamma = 0$ and $Fr \neq 0$ show that C_r and C_α do not depend on Fr in the studied range ($Fr < 0.1$). Using the results of the simulations at $Fr = 0$ (Eq. 3), we derive a theoretical expression for C_α which depends on Γ:

$$C_\alpha(\Gamma) = \frac{2}{\pi}\left(M_0 + \frac{M_1 - M_0}{1 + \frac{\Gamma_0}{\Gamma}}\right). \qquad (7)$$

C_α is not constant contrary to previous studies [3, 5] and depends on Γ. The equation 5 implies that the drag force D_x is null when $Fr = 0$ regardless of the value of Γ, which is consistent with the results presented in Figure 3a. By implementing the expression of C_α in the expression of the measured drag force D_0 in the case $\Gamma = 0$ and $Fr \neq 0$, it is possible to propose an expression of C_r when $\Gamma = 0$:

$$C_r = \frac{2(D_0 - M_0)}{\pi}, \qquad (8)$$

which leads to $C_r \simeq 0.35$. It is now possible to implement the expressions of C_r and C_α into Eqs. 6 and 5 to

determine D_x and M_z. The black solid line on figure 4a (respectively 4c) shows the proposed analytical function of D_x (respectively M_z). We can see that the behavior matches the simulations very well. It is expected that accounting for the microcopic friction int he contact law between grains will slightly affect the values obtained. The small remaining offset probably comes from the assumptions of the coefficients C_r and C_α which may have more complex dependencies depending on Fr and Γ. Furthermore, since the local packing fraction variation has not been taken into account in the model, it may also modify these values.

VII. CONCLUSION

In this study, we are interested in the set of forces and torques acting on a cross-shaped intruder moving in a granular material subjected to gravity (along y-direction). The possible movements of this cross are horizontal translation (along x-direction), rotation (along z-direction) or a combination of these two movements. The translation is described by a translationnal Froude number Fr and the rotation by a rotationnal Froude number Γ. The forces measured on the intruder are the drag force D_x, the lift force L_y and the torque M_z.

In the case of pure translation ($\Gamma = 0$) and low Froude number ($Fr < 1$), we find the results of the usual cases presented in previous studies [18–23]. The set of results is summarized as a constant drag force $D_x = D_0$, a constant lift force $L_y = L_0$ and a null torque $M_z = 0$.

In the case of pure rotation ($Fr = 0$) for values of $|\Gamma| < 1$, the results show an evolution with Γ. Even if the drag force remains null $D_x = 0$, the lift force remains constant at $L_y = L_0$ and then increase with Γ. The torque exerted on the intruder is constant $M_z = M_0$ as long as Γ is small and then increases with Γ. The evolution of M_z can be described by a phenomenological law similar to $\mu(I)$ rheology.

The combination of rotation and translation is not limited to an addition and reveals new behaviours for these three quantities. When Γ is small, rotation has no effect and similar results to pure translation are found for drag force, lift force and torque. As Γ increases, the torque increases and the drag force decreases. By applying the Granular Resistive Force Rheory, it is possible to describe the evolutions of D_x and M_z with Γ in agreement with the simulation results. The lift force loses the constant behavior that was observed in pure translation and pure rotation. The lift force decreases toward a value close to zero or even negative. The minimum lift force is obtained for the case $\Gamma/(2Fr) \simeq 1$. This first study opens the way to other studies closer to the problems of animal locomotion where it would be relevant to consider movements such as translation with imposed rotation or translation with imposed rotation.

Finally, it would be necessary to characterize the grain flow around the intruder in this geometry. This would allow a better understanding of the origin and the mechanisms that cause the drop in lift during rotation combined with translation. Even if this study showed the existence of Γ_m value, its origin is not clear yet. The understanding of this flow, of the local stresses and deformations will allow a better control of the problem of grain flows around rigid and moving objects.

ACKNOWLEDGMENTS

We warmly thank Thomas Courteaux for preliminary numerical simulations.

[1] R. D. Maladen, Y. Ding, C. Li, and D. I. Goldman, Undulatory Swimming in Sand: Subsurface Locomotion of the Sandfish Lizard, Science **325**, 314 (2009).
[2] C. Li, T. Zhang, and D. I. Goldman, A terradynamics of legged locomotion on granular media, science **339**, 1408 (2013).
[3] T. Zhang and D. I. Goldman, The effectiveness of resistive force theory in granular locomotion, Physics of Fluids **26**, 101308 (2014).
[4] A. Hosoi and D. I. Goldman, Beneath our feet: strategies for locomotion in granular media, Annual Review of Fluid Mechanics **47**, 431 (2015).
[5] B. D. Texier, A. Ibarra, and F. Melo, Helical locomotion in a granular medium, Physical review letters **119**, 068003 (2017).
[6] J. Uehara, M. Ambroso, R. Ojha, and D. J. Durian, Low-speed impact craters in loose granular media, Physical Review Letters **90**, 194301 (2003).
[7] H. Katsuragi and D. J. Durian, Unified force law for granular impact cratering, Nature physics **3**, 420 (2007).
[8] A. Seguin, Y. Bertho, and P. Gondret, Influence of confinement on granular penetration by impact, Phys. Rev. E **78**, 010301 (2008).
[9] A. Seguin, Y. Bertho, P. Gondret, and J. Crassous, Sphere penetration by impact in a granular medium: A collisional process, EPL **88**, 44002 (2009).
[10] T. A. Brzinski III, P. Mayor, and D. J. Durian, Depth-dependent resistance of granular media to vertical penetration, Physical review letters **111**, 168002 (2013).
[11] A. H. Clark, L. Kondic, and R. P. Behringer, Steady flow dynamics during granular impact, Physical Review E **93**, 050901 (2016).
[12] S. Athani and P. Rognon, Inertial drag in granular media, Physical Review Fluids **4**, 124302 (2019).
[13] D. Chehata, R. Zenit, and C. R. Wassgren, Dense granular flow around an immersed cylinder, Phys. Fluids **15**, 1622 (2003).

[14] A. Seguin, Y. Bertho, P. Gondret, and J. Crassous, Dense granular flow around a penetrating object: Experiment and hydrodynamic model, Phys. Rev. Lett. **107**, 048001 (2011).

[15] A. Seguin, Y. Bertho, F. Martinez, J. Crassous, and P. Gondret, Experimental velocity fields and forces for a cylinder penetrating into a granular medium, Phys. Rev. E **87**, 012201 (2013).

[16] M. B. Stone, R. Barry, D. P. Bernstein, M. D. Pelc, Y. K. Tsui, and P. Schiffer, Local jamming via penetration of a granular medium, Phys. Rev. E **70**, 041301 (2004).

[17] Z. Peng, X. Xu, K. Lu, and M. Hou, Depth dependence of vertical plunging force in granular medium, Phys. Rev. E **80**, 021301 (2009).

[18] I. Albert, P. Tegzes, R. Albert, J. G. Sample, A. L. Barabási, T. Vicsek, B. Kahng, and P. Schiffer, Stick-slip fluctuations in granular drag, Physical Review E **64**, 031307 (2001).

[19] Y. Takehara, S. Fujimoto, and K. Okumura, High-velocity drag friction in dense granular media, EPL **92**, 44003 (2010).

[20] D. J. Costantino, J. Bartell, K. Scheidler, and P. Schiffer, Low-velocity granular drag in reduced gravity, Phys. Rev. E **83**, 011305 (2011).

[21] J. E. Hilton and A. Tordesillas, Drag force on a spherical intruder in a granular bed at low froude number, Phys. Rev. E **88**, 062203 (2013).

[22] Y. Takehara and K. Okumura, High-Velocity Drag Friction in Granular Media near the Jamming Point, Phys. Rev. Lett. **112**, 148001 (2014).

[23] A. Seguin, Hysteresis of the drag force of an intruder moving into a granular medium, The European Physical Journal E **42**, 13 (2019).

[24] L. Huang, X. Ran, and R. Blumenfeld, Vertical dynamics of a horizontally oscillating active object in a two-dimensional granular medium, Physical Review E **94**, 062906 (2016).

[25] T. Faug, Macroscopic force experienced by extended objects in granular flows over a very broad froude-number range, The European Physical Journal E **38**, 1 (2015).

[26] A. Seguin, A. Lefebvre-Lepot, S. Faure, and P. Gondret, Clustering and flow around a sphere moving into a grain cloud, Eur. Phys. J. E **39**, 1 (2016).

[27] Y. Ding, N. Gravish, and D. I. Goldman, Drag induced lift in granular media, Physical Review Letters **106**, 028001 (2011).

[28] F. Q. Potiguar and Y. Ding, Lift and drag in intruders moving through hydrostatic granular media at high speeds, Physical Review E **88**, 012204 (2013).

[29] F. Guillard, Y. Forterre, and O. Pouliquen, Depth-independent drag force induced by stirring in granular media, Phys. Rev. Lett. **110**, 138303 (2013).

[30] F. Guillard, Y. Forterre, and O. Pouliquen, Lift forces in granular media, Physics of Fluids **26**, 043301 (2014).

[31] B. Debnath, K. K. Rao, and P. R. Nott, The lift on a disc immersed in a rotating granular bed, AIChE Journal **63**, 5482 (2017).

[32] S. Kumar, M. Dhiman, and K. A. Reddy, Magnus effect in granular media, Physical Review E **99**, 012902 (2019).

[33] C. S. O'Hern, S. A. Langer, A. J. Liu, and S. R. Nagel, Random packings of frictionless particles, Physical Review Letters **88**, 075507 (2002).

[34] C. S. O'Hern, L. E. Silbert, A. J. Liu, and S. R. Nagel, Jamming at zero temperature and zero applied stress: The epitome of disorder, Physical Review E **68**, 011306 (2003).

[35] G. MiDi, On dense granular flows., European Physical Journal E–Soft Matter **14** (2004).

[36] P. Jop, Y. Forterre, and O. Pouliquen, A constitutive law for dense granular flows, Nature **441**, 727 (2006).

[37] A. Seguin, C. Coulais, F. Martinez, Y. Bertho, and P. Gondret, Local rheological measurements in the granular flow around an intruder, Phys. Rev. E **93**, 012904 (2016).

[38] I. Albert, J. G. Sample, A. J. Morss, S. Rajagopalan, A.-L. Barabási, and P. Schiffer, Granular drag on a discrete object: Shape effects on jamming, Physical Review E **64**, 061303 (2001).

[39] S. Agarwal, C. Senatore, T. Zhang, M. Kingsbury, K. Iagnemma, D. I. Goldman, and K. Kamrin, Modeling of the interaction of rigid wheels with dry granular media, Journal of Terramechanics **85**, 1 (2019).

[40] S. Agarwal, A. Karsai, D. I. Goldman, and K. Kamrin, Surprising simplicity in the modeling of dynamic granular intrusion, Science Advances **7**, eabe0631 (2021).